Strategies for containing an emerging influenza pandemic in SE Asia.

Supplementary Information

Neil M. Ferguson[1], Derek Cummings[2] Simon Cauchemez[3], Christophe Fraser[1], Steven Riley[4], Aronrag Meeyai[1], Sopon Iamsirithaworn[5] & Donald Burke[2]

[1]*Department of Infectious Disease Epidemiology, Faculty of Medicine, Imperial College London, St Mary's Campus, Norfolk Place, London W2 1PG, UK*

[2] *Department of International Health, Johns Hopkins Bloomberg School of Public Health, 615 North Wolfe Street, Baltimore, Maryland, 21205, USA*

[3] *INSERM U707, 27 rue Chaligny, Paris, 75571 cedex 12, France*

[4] *Department of Community Medicine, 5/F William M.W. Mong Block, Faculty of Medicine Building, 21 Sassoon Road, Hong Kong*

[5]*Bureau of Epidemiology, Department of Diseases Control, Ministry of Public Health, Tivanonda Road, Nonthaburi 11000, Thailand*

Contents

1. Population data

Population density data

The 2003 Landscan[1] dataset prepared by Oakridge National Laboratory (see Figure SI1 below) was used as the source of population density information for SE Asia. This dataset has a 30 arc second resolution, equating to approximately 0.9km for Thai latitudes. The dataset is a model of population density which is constructed from census, remote sensing, land use and transport network data. It is a model of instantaneous population density (i.e. where people are at an instant of time) rather than residential population density, but for much of the world there is no better source for either instantaneous or residential density data (a notable exception being the UK, where census data provides sub-km resolution residential population data).

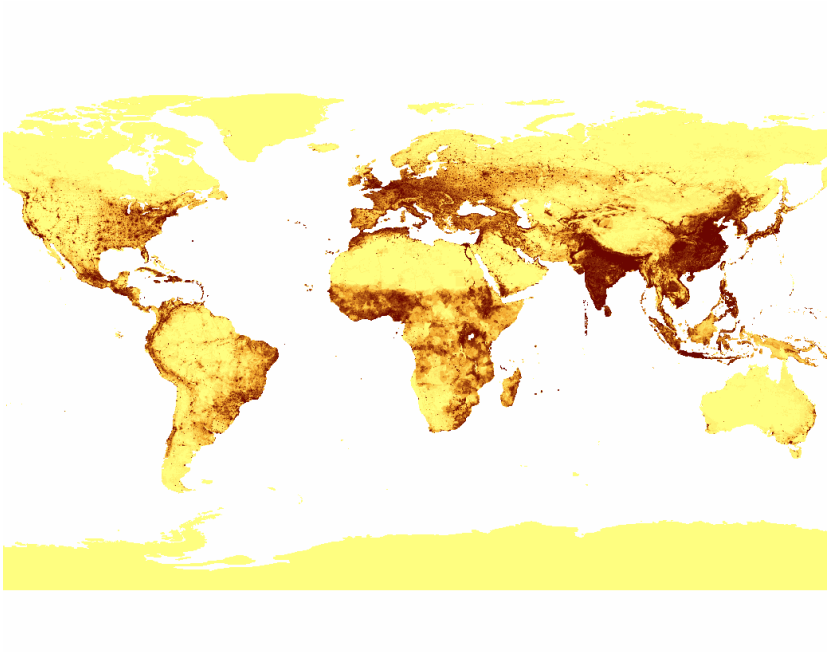

Figure SI1: Landscan 2003 [1] global population density dataset, with population density plotted on a logarithmic scale (lighter areas have lower density).

We modelled transmission within a area restricted to Thailand and a 100km buffer zone around its land borders (which included portions of Cambodia, Laos, Malaysia and Myanmar). The total population in this region was 85.84 million. No demographic, educational or travel-related data were available for countries other than Thailand, so we assumed Thai parameters across the modelled region.

Household size and age structure data

The sources for these data[2,3] are detailed in the main text. Here we note that it is not straightforward to construct a realistic demographic model of households which matches marginal distributions of household size and population age structure. Randomly assigning ages within households produces consistent marginal distributions but fails to capture a realistic generational-based age structure within households (i.e. households of 4 people tend to have 2 parents and 2 school-age children in, not 4 people with randomly selected ages). We therefore developed a rather heuristic model which maintained generational age gaps with households while matching overall household size and age distributions.

School size data and school allocation model

It is worth noting that the Thai school system differs from that commonly adopted in Europe and the US: as well as schools which are solely elementary (4-12 years, including a pre-school year) and secondary schools (12-18), a substantial proportion of schools are combined elementary and lower-secondary schools (i.e. include the 4-12 year and 12-15 year age groups, but not 15-18 year olds). These 3 school types were explicitly represented in the model.

Data on school attendance as a function of age was derived from Thai National Statistical Office data on school attendance and population size[2,4], and is plotted in Figure SI2 below.

Data on school sizes was obtained for a sample of 24,000 schools in Thailand[5], roughly 2/3 of all schools in the nation. This sample was patchy in its spatial coverage, however – with only approximately 60% of provinces being included. Distributions of school types and sizes did not vary widely by province, but we were not able to verify anecdotal reports that combined elementary+secondary schools were more common in rural areas from the district-level stratification the sample provided. We therefore assumed no geographic variation in the distribution of school types. Overall, 41,700 primary schools, 12,500 elementary+secondary schools, and 6,900 secondary schools were modelled, with average sizes of 175, 420 and 750 pupils respectively.

The simulation locates schools randomly across the modelled region with a probability proportional to the population density, the total number of schools being selected to give the correct average size for each type of school at a national level. Pupils are then allocated to schools using a free selection algorithm; each child 'picks' a school at random from the nearest 3 (for elementary or elementary+secondary school types) or 6 schools of the appropriate type, with a probability weighted by the distance kernel derived from the Thai National Migration Survey data on commuting behaviour (see below). Restricting school choice to the nearest 3 or 6 schools avoids unrealistic long tails to the distribution of distances travelled to school, and matches other data on the average distance travelled to elementary and secondary schools[6]. The allocation algorithm matches observed distributions of schools sizes reasonably well, and predicts (in agreement with anecdote) that small schools will typically be found in low population density (i.e. rural) areas.

Lower-secondary age students are allocated to combined elementary+secondary or pure secondary schools with probabilities determined by the observed proportions of such children attending each school type.

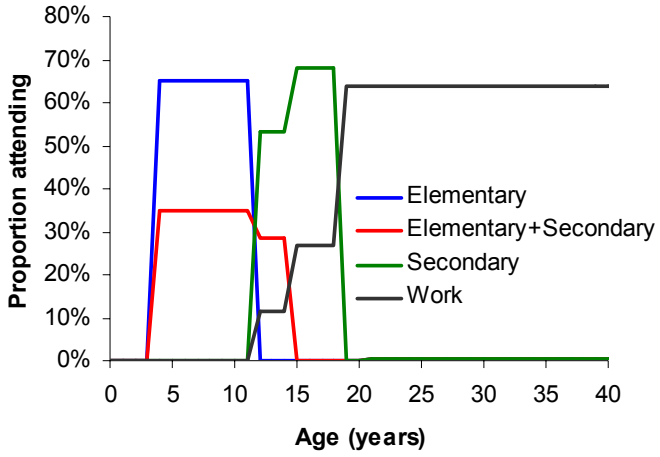

Figure SI2: Proportion of population attending different school types and travelling to a workplace in Thailand as a function of age. Trends are constant for ages 21-75. Those over 75 are assumed not to travel to work. Those working at home are not included in the figures for Work above. Adults shown as attending the different school types are teachers.

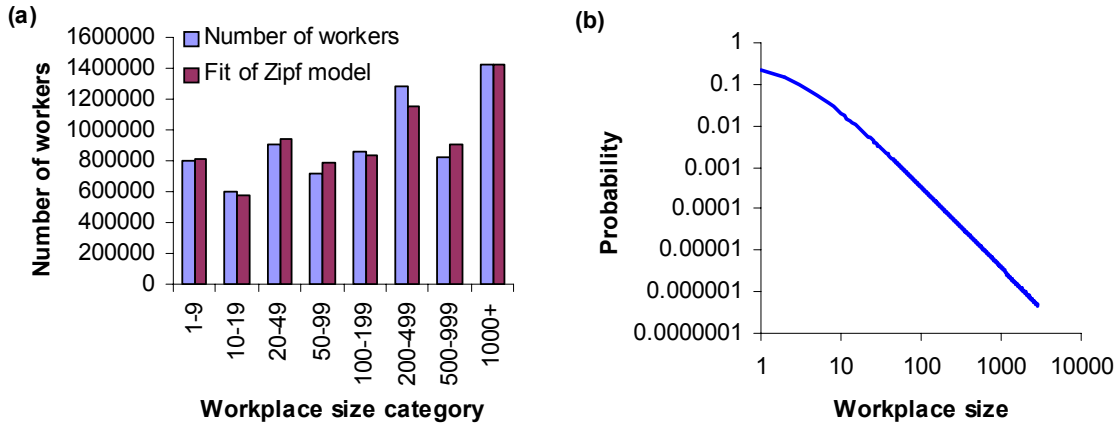

Figure SI3: (a) Data on numbers of workers in Thailand working in workplaces of different size categories[7], compared with maximum likelihood fit of Zipf model for workplace size distribution. (b) Best fit probability distribution of workplace sizes.

Workplace data and allocation model

Like those of most countries[8], Thai workplaces obey a power law distribution for the number of employees. Data on numbers of workplaces by size is provided in size groupings: we fitted this categorical distribution to a discrete power-law distribution using maximum likelihood methods by integrating over each size category. The resulting workplace size distribution has Zipf-like form (namely an offset truncated power distribution)

$P(n>m)=\left(\left[\left(1+m_{\max}/a\right)/\left(1+m/a\right)\right]^{c}-1\right)\Big/\left[\left(1+m_{\max}/a\right)^{c}-1\right]$ for $m \leq m_{\max}$ with parameter estimates a= 3.26, c=0.97 and $m_{\max}$=2870 (see figure SI3).

The algorithm to allocate individuals to workplaces was necessarily more complex than the school allocation algorithm – while the school size distributions could be approximately matched with a 'free choice' algorithm, the highly over-dispersed workplace size distribution requires constraints on workplace choice to be imposed. The challenge in developing an algorithm which matches both workplace size data and the observed distribution of distances travelled to work is one of computational efficiency – it is very easy to find algorithms which are $O(N^2)$ and take days to allocate large populations. We developed a probabilistic dynamical algorithm based around the concept of workers competing for available vacancies with a choice function which depended on distance from household location (the 'choice kernel'). A full description is beyond the scope of this paper, but the result was non-biased and met the marginal distributional constraints on commuting distribution distance (see Fig 1 of main text) and workplace size.

Travel data

A survey of migration in Thailand performed by the Institute for Population and Social Research at Mahidol University asked the employed and student members of 7537 households whether their workplace or school was in the same district in which they lived, and how far they travelled to get there[9]. For those members who worked or attended school within the same district in which they lived, this distance was not reported. This necessitated adjusting the reported commuting distance distribution to correct for this form of short-distance censoring.

There were 2517 respondents in total, of whom 2081 (83%) reported their school or workplace was in their residential district provided an estimate in kilometres of the distance to their

workplace or school. Of the 436 who worked or went to school out of district, 305 reported the distance they travelled to work.

To estimate the distance travelled to school/work for the population as a whole from distance data for those working in different districts, one needs to calculate the probability that a journey of a given distance will be to a point outside the district of residence. Since data on the district of residence was not available for respondents, we made the simplifying assumption that districts had been sampled randomly, and that to a first approximation districts could be considered as circles of uniform population density. Given a point randomly selected from within a unit radius circle, we then calculated the probability $p(x)$ that a second randomly selected point a distance x from the first point would also lie within the same circle (Figure SI3a). Then given the probability distribution that a district will have mean radius r (Figure SI3b), $z(r)$, the probability that a workplace distance L from a household will lie within the district of residence can be approximated by (see top curve of Figure SI3c)

$$q(L) = \int_0^\infty p(L/r)z(r)dr$$

If $g(L)$ is the reported distribution of journey lengths outside the district of residence, then the expected distribution of all journey lengths, $h(L)$, is just proportional to $g(L)/[1- q(L)]$ (see middle curve of Figures SI3c). However, this assumes no bias towards picking workplaces within one's district of residence. In reality, natural boundaries and heterogeneous population density might be expected to invalidate this assumption - and indeed, the predicted proportion of within-district journeys using $h(L)$ is just 71%. Given s (=0.83), the observed proportion of within-district journeys, we can simply correct for this discrepancy by increasing the proportion of within-district journeys, thus deriving a final distance distribution $u(L)$ corrected for censoring and a within-district bias (lower curve of Figure SI3c):

$$u(L) \sim g(L)\left(1+\frac{q(L)}{1-q(L)}\frac{s}{1-\int_0^\infty \left(g(L)\Big/[1-q(L)]\right)dL}\right)$$

We fitted the simulated distribution of distance of journeys to work from the model to this corrected distribution of commuting distances assuming an offset power-law 'choice' kernel for movements (i.e. people pick from the set of all workplaces with a probability weighted by distance D using the choice kernel $f(D)$) [See Methods in main text].

In the absence of other data, we used the kernel thus derived for both journeys to work/school, and random travel ('community' transmission). Relative contact rates for community transmission (defined by parameter $\varsigma(a_i)$) associated with non-work travel was assumed to vary with age, being fixed at 100% for ages 20-65, 75% for age bands 15-20 and 65-70, 50% for age bands 10-15 and 70-75, 25% for age bands 5-10 and 75-85 and 10% for age band 0-5. However, this reduction in travel related contact rates for low and high ages had little impact, with similar results being obtained if constant contact rates for all ages were assumed.

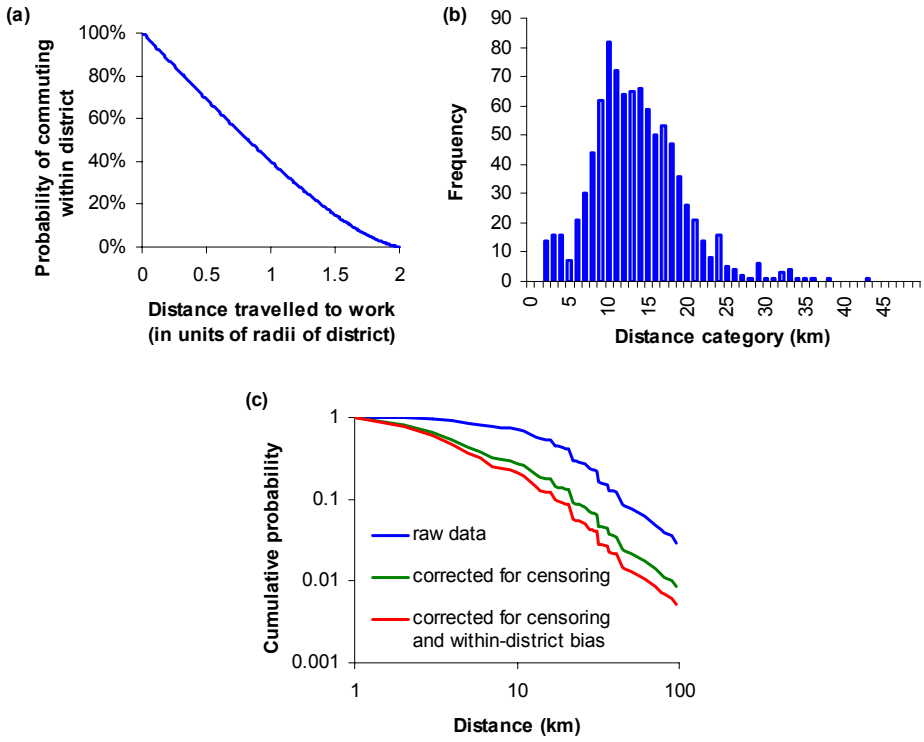

Figure SI3: (a) Probability of commuting within district as a function of distance travelled in units of the district radius, and making the simplifying assumption that the direction of travel is random and that districts are is circular. (b) Frequency distribution of the mean radius (in 1km categories) of the 889 districts in Thailand, calculated from boundary data (c) Cumulative probability of travelling over a certain distance to work. The raw National Migration Survey data is shown (n=305), together with the distributions corrected for censoring of within-district journeys and for censoring plus the observed bias to work within the district of residence.

2. Modelling details

Details of the transmission model

The model is a stochastic, spatially structured individual-based simulation. We consider transmission occurring in a population of size N resident is a geographic region denoted Ω. Given an empirical population density function, $\rho(\mathbf{r})$ defined on Ω (where $\mathbf{r}$ is the coordinate vector of a point in Ω), the model generates a simulated population such that the population of any subset of Ω is given by $N_{\omega\subset\Omega} \sim \text{Poi}\left(\int_{\omega} \rho(\mathbf{r})\, d\mathbf{r}\right)$. An individual i in the population is defined by their age, a_i, household membership, h_i, and place membership, l_i^j. Individuals are co-located in households, with households being constructed to reflect typical generational structure while matching empirical distributions of age structure and household size for Thailand (Figure 1b,c). There are n_p place types, denoted $j = 1..n_p$. We assumed $n_p = 4$ here, with types 1 to 4 representing pure elementary schools, mixed elementary and lower secondary schools, pure lower and higher secondary schools, and workplaces respectively. The proportions of individuals attending different place types varies by age (see Section 1 above), and we assumed individuals are members of only one place. Places are distributed randomly in space, with a density proportional to that of the population. Individuals are randomly allocated to places at the start of a

simulation, with a probability which can depend on the distance between the individual and place and the number of individuals the place still has space for. Individuals are always allocated to places in the same country as their household location. For place types 1..3 (schools), only the total number of places of each type is constrained (thus constraining mean place size) – no constraint on the maximum membership of any one school is imposed. For place type 4 (workplaces), membership is constrained to produce a distribution of workplace sizes which matches the data discussed above, while also reproducing the observed distance to work distribution for Thailand. We define n_i and m_i^j as the number of people in the household and place type j of individual i respectively.

Defining $I_i = 1$ if individual i is infectious and 0 otherwise, $C_i = 1$ if individual i is a severe infection (50% of infections are assumed to be severe, with C_i being randomly assigned for each new infection as 0 or 1), and τ_i to be the time host i became infectious, the force of infection experienced by individual i, λ_i is then given by

$$\lambda_i = \sum_{k|h_k=h_i} \frac{I_k \beta_h \kappa(t-\tau_k)\rho_k\left[1+C_k(\omega-1)\right]}{{n_i}^{\alpha}} + \sum_{j,k\left|l_k^j=l_i^j\right.} \frac{I_k \beta_p^j \kappa(t-\tau_k)\rho_k\left[1+C_k\left(\omega\psi_p^j(t-\tau_k)-1\right)\right]}{m_i^j} + \frac{\sum_k I_k \varsigma(a_i)\beta_c \kappa(t-\tau_k)\rho_k f\left(d_{i,k}\right)\left[1+C_k(\omega-1)\right]}{\sum_k f\left(d_{i,k}\right)}$$

Here k indexes individuals in the population, j indexes place types. β_h, β_p^j and β_c are transmission coefficients for household, place and community transmission respectively, α (=0.8) is a power determining the scaling of household transmission rates with household size, and ω (=2 – in line with the analysis of household data presented below) is the infectiousness of a severe infection relative to a mild one. ${\psi_p}^j(x)$ (=0.1, 0.2, 0.25 and 0.5 for j=1,..,4 respectively for x>0.25 days and 0 otherwise) is the factor by which within-place contact rates change for symptomatic severe infection (reflecting sickness-induced absenteeism) as a function of time since onset of infectiousness, $f\left(d_{i,k}\right)$ is the value of the spatial kernel function at the distance $d_{i,k}$ between individuals i and k (this represents a form of gravity model[10,11]), and $\varsigma(a_i)$ is the relative travel-related contact rate of an individual of age a_i (see Section 1 above). We assume severe infections are detectable a minimum of 0.25 days after infectiousness start (*i.e.* after the latent period ends).

While the baseline results in the main text assume no variation in infectiousness between individuals, the model allows for variation, since ρ_k – the relative infectiousness of individual k – can be picked from a gamma distribution with mean 1. Sensitivity analysis to the value of k is given in section 4 below.

Bayesian likelihood-based analysis of household infection data (see section 3 below), gave β_h=0.47/day (corresponding to a within-household R_0 of 0.6) for an overall R_0 of 1.8. We partition non-household transmission to give levels of within-place transmission comparable with household transmission (i.e. $R_0 \approx 0.6$ for each type of transmission) and to qualitatively match 1957 pandemic age-specific attack rates. This gave β_p^j=0.94/day for j=1..3, β_p^4=0.47/day and

β_c=0.075/day for R_0=1.8. R_0 was calculated numerically as the equilibrium average per-generation reproduction number in the exponential growth phase of the epidemic (typically infection generations 4 to 8). When varying R_0, all transmission coefficients were varied by the same factor.

Seasonality

We did not include seasonality in transmission in the model; it is unclear what affect seasonality might play in pandemics, but while it may partly explain the 'waves' seen in past pandemics in temperate climates, the limited seasonal variation in transmission of interpandemic flu seen in tropical countries[12,13] suggests seasonality – while present – is likely to be less important in the setting of Thailand.

Mortality/morbidity

We did not model disease-related mortality here as we were principally interested in policies aimed at containing spread rather than minimising mortality/morbidity – though of course, successful containment can be expected to dramatically lower both the national and global health burden any emergent pandemic.

Numbers of realisations

For any stochastic model, it is essential to undertake sufficient realisation to ensure ensemble behaviour is well characterised for any one set of parameter values. When estimating the probability of elimination for a particular control strategy, the computational burden associated with realisations where control fails are many-fold larger than for realisations where the infection goes extinct. To optimise both estimation accuracy and computational efficiency we therefore stopped generating realisations when either 1000 had been generated in total, or when 50 (or 200 when estimating extinction probabilities in the absence of controls) realisations in which control failed had been generated, whichever happened first. The error in estimates of the proportion of realisations in which extinction occurred was therefore negatively binomially distributed, and was rather larger for low compared with high (>80%) probabilities of extinction (see errors on figures showing probabilities of elimination in main text).

To estimate the proportion of realisations which go extinct under a particular control policy but would have been large otherwise, we independently estimated the probability of elimination with and without the control policy (for the same values of other parameters). Denoting these probabilities p_c and p_n respectively, the proportion of otherwise large outbreaks which are contained by the control policy is then estimated as $1-(1-p_c)/(1-p_n)$. The mean number of courses required to contain an otherwise large outbreak is calculated likewise, with the (largely accurate) assumption that antiviral usage for outbreaks which spontaneously go extinct is negligible. Overall ~200,000 model realisations were performed for the results presented in this paper.

3. Natural history parameters

Past modelling studies have largely assumed distributions of the incubation and infectious periods first reported in two historical papers[14,15]. However, the primary data for these estimates (in particular, those used to estimate the duration of infectiousness) are lacking. We therefore derived new estimates of the incubation period and development of infectiousness over time for human influenza from available primary data.

Estimation of latent period

We estimated the incubation period (time from infection to the start of symptoms) distribution for human influenza from (fairly unique) data on a multiple exposure event occurring on an aeroplane[16], in which 37 people were infected by a single person on the same relatively short flight. The delay from exposure to onset of symptoms was reported to the nearest half-day (see Fig SI5). The best maximum likelihood fit to this data was given by a right-shifted Weibull distribution with a fixed offset of 0.5 days, power parameter 2.21 (95% CI: 1.36-3.37) and scale parameter 1.10 (95% CI: 0.83-1.42) – giving a mean incubation period of 1.48 days and standard deviation of 0.47 days.

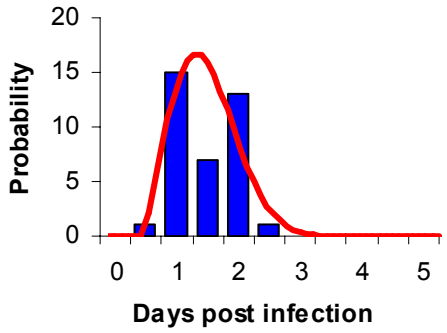

Figure SI5: Incubation period data[16] and best fit to offset Weibull distribution.

Estimation of infectiousness over time

Building on past work[17], we reanalysed data from a study of influenza infections in households[18] which involved the daily follow-up of influenza symptoms in household members for the 15 days after an index case visited a general practitioner. 334 households had an index case with virologically confirmed influenza.

In modelling infection in households, we assumed that individuals in the household could be infected from outside the household at rate α, or from within the household. Since 79 households had at least 2 cases with symptoms at day 0 (day when the index case went to the general practitioner), the statistical framework allowed co-primary infections as follows: given a first infection had occurred in the household, other members of the household could have been infected at the same time with a probability p.

A subject was successively susceptible, infected but not infectious (latent), and infectious. We assumed (see above) that (a) the latent period had a Weibull distribution (2.24, 1.11) with offset 0.5 day and density $h(.)$, and (b) infectiousness and symptoms began at the same time (though in the full model of transmission in Thailand, we assume a minimum of a 0.25 day delay from the onset of symptoms to the earliest time individuals might notify healthcare services).

After the end of the latent period, infectiousness in an individual was assumed to change over time, with the profile of infectiousness being given by a function $\kappa(T)$ where T is the time elapsed from the end of the latent period. We assumed $\kappa(T)$ had a lognormal form $\kappa(T;\delta,\gamma)$ where δ and γ are the mean and standard deviation of $\ln(T)$. We truncated this distribution at 10 days since given the 14 day followup time in this study, infectiousness cannot be reliably estimated beyond 10 days. Furthermore, it is biologically unrealistic to use a non-truncated distribution, as the great majority of people recover from infection within 10 days.

Once a case was infectious, the force of infection to other household members is given by:

$$\lambda(T) = \beta\kappa(T;\delta,\gamma)/n^{0.8}$$

where β is the infectiousness parameter. A dependence of the force of infection on the size n of the household of the form $n^{0.8}$ provided the best fit with observed data[17]. Note that the probability that a household member has escaped infection T days after the case became infectious is $B(T) = \exp\left(-\int_0^T \lambda(u)du\right)$.

It is interesting to speculate on the causes for the perhaps unexpected dependence of λ on n: it may reflect a transmission contact process which is highly intermittent; so that infected individuals do not pose a continuous infection hazard to household members, but rather only pose a risk during certain infrequent and well-defined close-contact event which is only ever likely to infect 1 person (e.g. sneezing when very close to another household member). The infection risk might then be very different even for household members in the same room as an infected individual, making dynamics closer to mass-action due to infectious events being partitioned between household members.

A score S_c was defined for the severity of symptoms (proportion of 13 clinical symptoms reported on the first day of illness). Denoting m its median value among contact cases, a case was considered as "severe" when $S_c > m$, and as "non-severe" otherwise. Due to inclusion criteria to participate in the study[18], almost all index cases were found to be severe. The infectiousness parameter β was estimated separately for severe and non-severe cases.

Data augmentation Markov chain Monte Carlo (MCMC) techniques were used to deal with missing data[17]. For each case i, the data were augmented with 1) the exact time ν_i of infection, and 2) the exact time ζ_i when infectiousness (and symptoms) started. The framework ensured that augmented data were consistent with observed data.

In a household of size n, given the augmented data, the time of the first infection ν_m and the number k of co-primary cases were available. Denoting I the set of cases, the contribution of non co-primary case i to the likelihood was:

$$(1-p)\exp\{-(\upsilon_i-\upsilon_m)\alpha\}\left\{\prod_{j\in I-\{i\}} B(\upsilon_i-\zeta_j)\right\}\left\{\alpha+\sum_{j\in I-\{i\}}\lambda(\upsilon_i-\zeta_j)\right\}h(\zeta_i-\upsilon_i)$$

where the first term is the probability that case i is not a co-primary case; the second and third terms are the probabilities that case i has escaped to community and within-household transmission up to time ν_i; the fourth term is the instantaneous risk of infection at time ν_i; and the last term is the density of the latent period. Similarly, the contribution of a subject that was not infected during the 15 days follow-up was:

$$(1-p)\exp\{-(15-\upsilon_m)\alpha\}\left\{\prod_{j\in I} B(15-\zeta_j)\right\}$$

For the remaining k co-primary cases, it was:

$$p^{k-1}\prod_{i\in I^*} h(\zeta_i-\upsilon_i)$$

where I^* is the set of co-primary cases.

Flat Exponential *priors* with parameter 0.001 were specified for parameters α, β and γ; Uniform *priors* were specified for p (U[0,1]) and δ (U[-10,10]). The joint *posterior* distribution of augmented data and parameters was explored by Metropolis-Hastings MCMC sampling [17]. We

performed 1,000,000 iterations. The first 10,000 were discarded as the burn-in period. The output was then recorded one every 10 iterations to constitute a sample from the *posterior* distribution. The convergence of the MCMC was visually assessed.

Table SI1 presents *posterior* means and 95% credible intervals of the parameters.

Parameter	*Posterior* mean	95% credible interval
p (%)	8.5	5.1, 12.2
α (10^{-3} day^{-1})	6.0	2.2, 10.4
β_{Severe} (person$^{0.8}$ day^{-1})	0.88	0.72, 1.04
$\beta_{\text{Non-severe}}$ (person$^{0.8}$ day^{-1})	0.49	0.09, 1.13
δ (log(day))	-0.72	-1.64, -0.09
γ (log(day))	1.8	1.3, 2.5

Table SI1: *Posterior* means and 95% credible intervals of the parameters.

From these values, the posterior mean estimate of the generation time, T_g, is 2.6 days (95% credible interval= 2.1-3.0 days).

Ongoing work will examine the consistency of these estimates with published case-to-case interval data from other household studies. Such analyses are required to rule out the possibility that the comparatively short generation time estimate we obtained above may not be representative of typical transmission events in the community. A variety of mechanism which might generate such biases can be hypothesised (e.g. pre-existing immunity may have shortened the period of shedding for the French household study, or household contacts involving clinical cases are more intimate, perhaps permitting transmission at an earlier stage than in the community), and while most are perhaps unlikely, a second independent estimate of T_g would be ameliorate such concerns.

Transmission parameters and estimation of R_0 for influenza

The estimates of δ and γ were used directly to derive the infectiousness profile used in the simulation model. The estimates of β were used as guides, but in addition to fitting to the household data set presented above, we also optimised the values used in the simulation to fit a subset of household infection data from the Tecumseh study reported by Longini[19]. The data subset used was the infection rates in a season in households where all household members had a 'low' antibody titre to influenza at the start of the season.

Fitting to this additional dataset enables the ratio of within-household to between-household transmission to be estimated, since the dataset reports the proportion of households where no infection was detected. In fitting to this dataset, we used the estimates of population immunity reported in that paper which correspond (crudely) to assuming that 27% of the population is immune at any one time. We assumed immunity was clustered in households and therefore initialized simulations of that dataset by making all members of 27% of households (randomly selected) immune, and assuming complete susceptibility in the remainder. The best fit of the simulation model to the 2 household datasets (Figure SI6) gave a within-household β of 0.47 for non-severe cases (assumed to be 50% of all infections) and we assumed a 2-fold higher infectiousness for severe cases (namely β=0.94 – well within the 95% credible interval given in table SI1). Within-household transmission was estimated to be 1/3 of all transmission and the best estimate of the R_0 of inter-pandemic influenza was 1.8.

This value of R_0 is also consistent with estimates derived from time-series data on influenza-related mortality in 1918-19 in both the US and UK (see Figure SI7 and Figure 1f in the main text). Recent estimates[20] of the R_0 of the 1918 pandemic strain were in the range 2-3, but these assumed a generation time of approximately 4 days. Reducing the estimate of T_g to 2.6 days reduces the estimates of R_0 obtained from epidemic growth curves accordingly.

In estimating R_0 from mortality curves, we calculated the running 2 week average gradient, *r*, and used the relation $R_0 \approx 1 + rT_g$. This relationship is approximate for non-exponentially distributed incubation periods, or for non-exponential changes in infectiousness over time, but we verified by simulation that the slight errors in R_0 estimates produced were minor compared with the within-city and between-city variation observed.

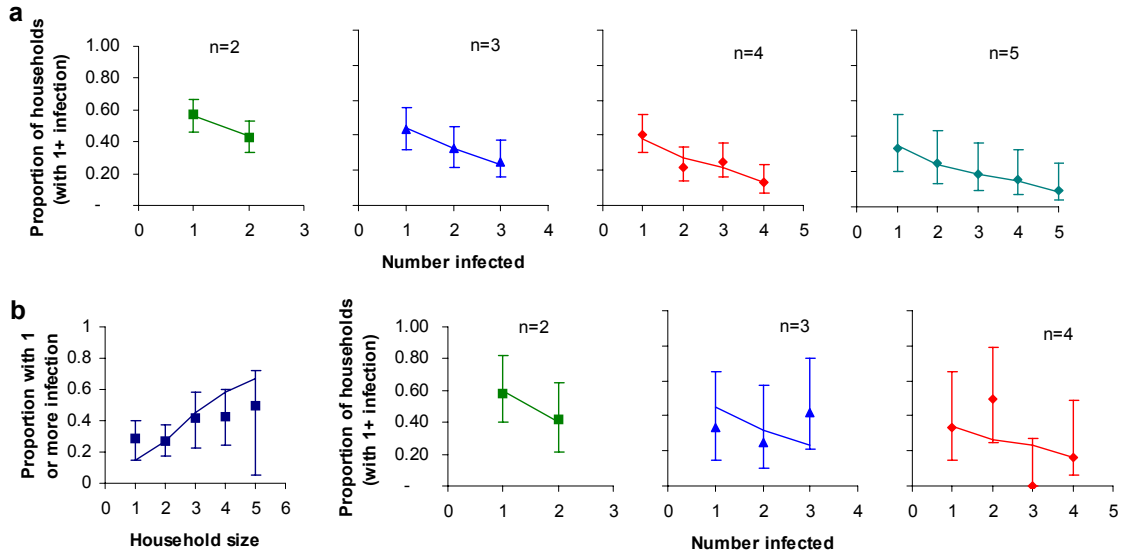

Figure SI6: Fit of simulation model (lines) to household datasets (points): (a) Number of infections observed in households over a 2 week period following reporting of an index case as reported by Cauchemez et al [17]. Proportion of households with 1 or more infection shown, and distributions of numbers of infections within a household conditional on 1 or more infections. To fit this dataset, infection was seeded at day zero in 100,000 randomly selected households, no between-household infection was modeled, and the simulation was run for 17 days (to allow for the incubation time of the index case). Additionally, we assumed the index case would be 'severe' – in line with the trends seen in the data (see above). (b) Number of infections observed in households of different sizes over a single season in the Tecumseh study [19]. To fit this data we assumed 27% population immunity (see discussion above), seeded the novel strain in 10 households on day 0, and ran the model for 300 days (between household transmission was modelled).

It is interesting to note the substantial variation in temporal incidence patterns in the 1918 pandemic in different US and British cities[20,21]. This and the multiple 'waves' of spread seen is suggestive that control measures (including spontaneous reductions in contact rates) may have had a significant impact on transmission. However, in the absence of quantitative data on the timing and intensity of controls imposed in different locations, the extent to which such variation can be attributed to differences in control measures (as compared with demographic or environmental stochasticity) can currently not be assessed.

R_0 =1.8 also gives a 50% infection attack rate in the simulation model – consistent with the (albeit limited) data on infection attack rates in the first year of past pandemics (Figure SI8). However,

the simulation does not include the effect of seasonal variation in R_0, the effect of which is unclear as yet, but may reduce overall pandemic attack rates somewhat.

It should also be noted that we assume no cross-protective immunity between one subtype and another, so the entire population is completely immune to any new pandemic strain. We similarly assume that the 'low-titre' households from the Tecumseh are completely susceptible. If these assumptions are incorrect (*i.e.* cross-protective immunity is be present in the absence of a significant antibody-mediated cross-protective response), then the 'fundamental' R_0 of influenza might be larger than estimated, since we would have really estimated the 'effective reproduction number', R – *i.e.* the rate of transmission measured in the presence of some immunity. However, such a bias might not affect conclusions about control policies for any new pandemic. If heterosubtypic cross-immunity was significant for past pandemics, we might also expect it to be so for any future pandemic – meaning the rate of spread would again be determined by the effective reproduction number measured from past pandemics, rather than the basic reproduction measure which would determine the rate of spread in a truly naïve population (*i.e.* one which had never been exposed to any form of influenza A).

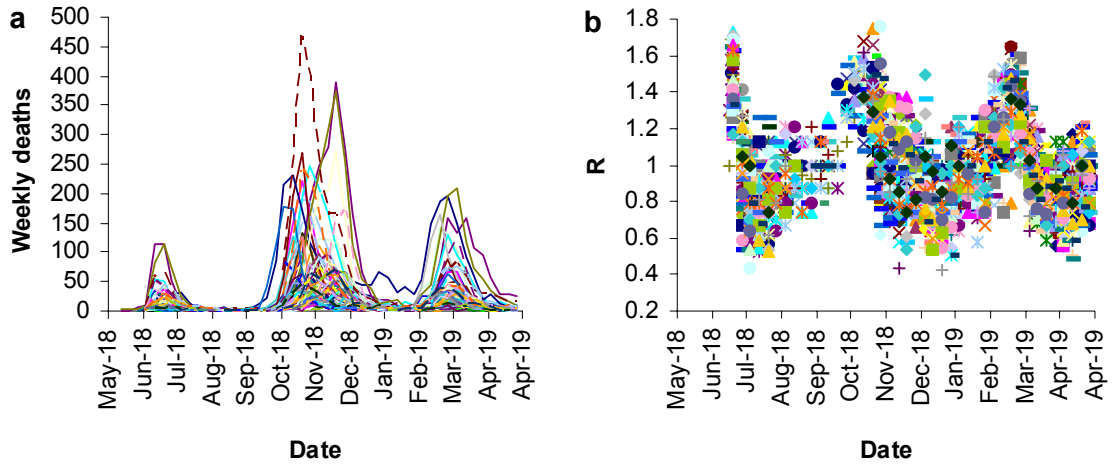

Figure SI7: (a) Excess weekly mortality in 83 British cities in 1918-19 [21]. (b) Corresponding weekly estimates of the effective reproduction number, *R*, derived (see text above) by calculating the running average slope calculated over a 2 week window from the data shown in (a). Estimates peak at 1.8 for a few cities, though are typically much lower.

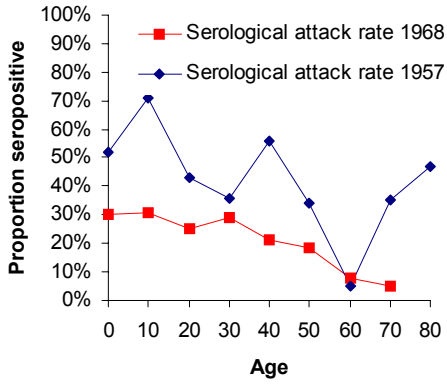

Figure SI8: Age-specific serological attach rates for the 1957 and 1968 pandemics[22].

4. Sensitivity analyses

Pure social targeting of prophylaxis

The least intensive prophylaxis policy we examine is social targeting - namely prophylaxing individuals in the same household, school or workplace as a newly diagnosed case Figure SI9 illustrates the impact of such a policy, as a function of how quickly the pandemic strain is detected and how rapidly drug is distributed. Elimination of the pandemic strain within 100 days has ≥90% probability for $R_0 \leq 1.6$, given (unrealistically) perfect surveillance and implementation (top curve of Fig SI9a). If successful, social targeting also requires limited drug stockpiles (Fig SI9b) - <50,000 courses on average, and <150,000 courses even in the most challenging scenarios (e.g. when the original cluster grows rapidly, perhaps due to emergence close to a urban centre), and eliminates the new strain after fewer than 150 cases have arisen.

If the original case cluster is only detected after 20 severe cases have arisen (reached by day 14 on average for $R_0 \sim 1.5$), policy effectiveness drop drastically, however (Figure SI9a) – but interestingly the additional fall in effectiveness caused by starting after 40 cases is relatively slight. Once the policy has been initiated, delays in detecting cases and/or prophylaxing the targeted population has an even more catastrophic effect on effectiveness – with a 2 day delay between case onset and prophylaxis containment is feasible only up to $R_0 \sim 1.25$ (Fig SI9f), and geographic spread is seen up to 50km (Fig SI9e) even when containment succeeds.

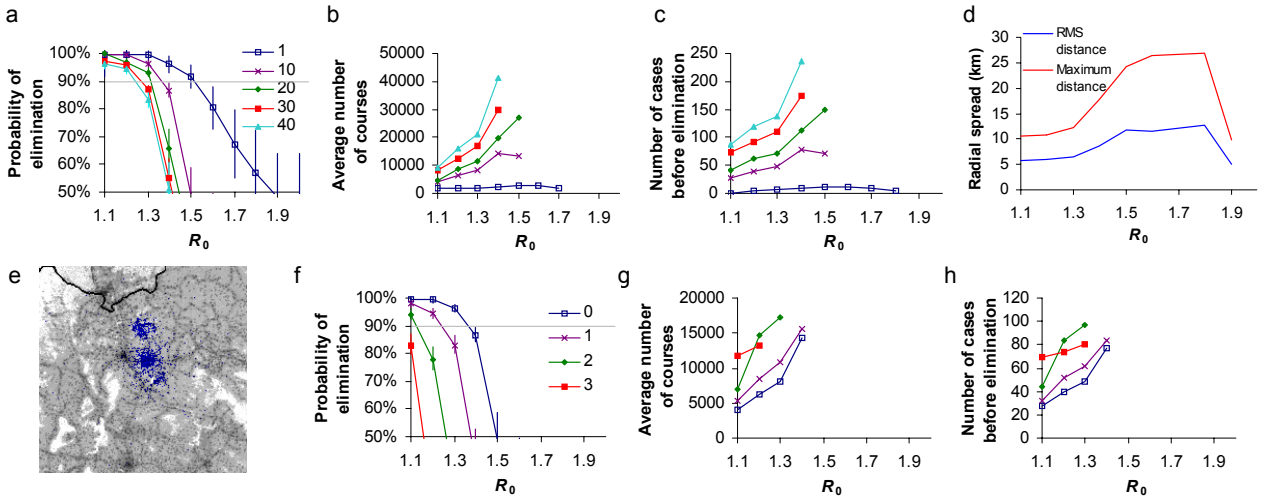

Figure SI9: Effectiveness of a policy of socially targeted antiviral prophylaxis, assuming 90% of severe cases are detected and prophylaxis of 90% of household members and 90% of pupils or colleagues in 90% of the schools or workplaces of detected cases. (a) Probability of eliminating an otherwise large epidemic within 100 days (results for longer time periods are virtually identical), as a function of R_0 of the pandemic virus (x-axis) and the number of (clinically severe) cases detected before the policy is initiated (the different lines). Results assume no delay in prophylaxis once a case is detected. (b) as (a) but showing average numbers of courses of drug required for successful containment of an otherwise large outbreak. (c) as (a), but showing the number of clinically severe cases arising before successful elimination occurs. (d) Root-mean-square (RMS) and maximum distance of spread (averaged across at least 50 realisations) of the epidemic from its seed location by the time it was eliminated from introduction as a function of R_0 for a policy assuming no delay to initiation of policy and no delay in prophylaxis after case detection. (e) Map (of 200x200km square of central north Thailand) showing extent of spread during one contained R_0=1.5 epidemic assuming a 2 day delay from case detection to prophylaxis and that policy initiated after 10 severe cases. Blue represents areas where treatment ahs occurred. Delays in prophylaxis weaken geographic containment. (f-h) as (a-c), but varying the number of days required from detection of a case to completion of prophylaxis and assuming policy starts after 10 severe cases detected. Policy efficacy becomes minimal for delays of over 1 day in detecting a case an implementing prophylaxis.

Time delays in starting policy

In the main text, we have concentrated on the scenario that the delay to initiating any control policy will be determined by the number of cases which have arisen from the primary cluster, rather than purely by chronological time. Figure SI10 shows that the effect of replacing a case number based starting threshold with a fixed time delay to policy initiation has little impact on policy conclusions. The 20 case threshold used for most results in the main text corresponds approximately to a 14 day delay in policy initiation, though of course there is considerable variability in the precise timing of policy initiation for a case threshold start criterion due to stochastic variability in the initial rate of growth of outbreaks.

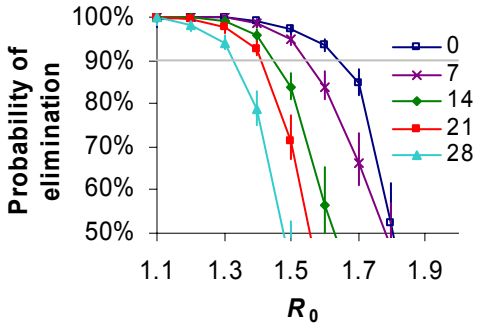

Figure SI10: Effect of a fixed time delay (measured in days) from the onset of the first case in the pandemic cluster to the initiation of a containment policy of socially targeted prophylaxis plus 5km radial prophylaxis with a 2 day delay from case onset to completion of prophylaxis in the population in the vicinity of each case. Other parameters as Figure 4d in main text.

Proportion of school/workplace vs community transmission

While data from household studies enables the relative levels of household and non-household based transmission to be estimated, we have much more limited information on which to base assumptions about the relative levels of transmission in workplaces/schools versus the community in general (i.e. random contacts). We therefore assumed levels of transmission were approximately equal in each context for the results in the main text (R_0 =0.6 in each context for a total R_0 of 1.8).

Figure SI11 shows the effect of varying that assumption on the effectiveness of a radial prophylaxis containment strategy: policy effectiveness is not significantly affected by small changes in the relative levels of transmission in each context, but if transmission in places is 4-fold lower than was assumed (the 25% curve), the effectiveness of geographically-targeted policies increases (since more transmission is purely spatial, in the vicinity of each new case). If the level of school/workplace transmission is 50% higher than assumed (the 150% curve), policy effectiveness declines, since social-targeting only treats the schools and workplaces of diagnosed cases - here assumed to be only 45% of all infections. Geographic targeting is less sensitive to the degree of case ascertainment due to the spatial clustering of new infections.

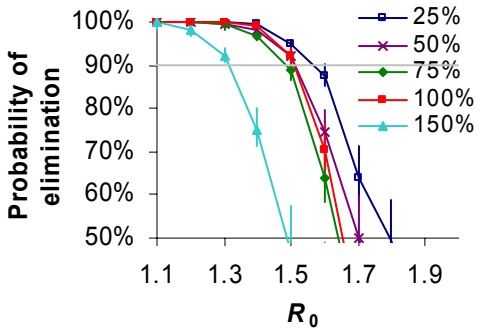

Figure SI11: Effect of varying the relative proportion of transmission occurring in schools and workplaces versus the community. 100% corresponds to the baseline (equal levels of transmission in each context). Results assume a 2 day delay from case onset to completion of prophylaxis in the population in the vicinity of each case.. Other parameters as Figure 4d in main text.

Heterogeneity in infectiousness

SARS highlighted the important role of heterogeneity in infectiousness (or contact rates) between individuals (the so-called 'super-spreader' events) in determining the pattern of spread in different locations. To investigate the possible significance of heterogeneity in infectiousness on pandemic containment, we allowed individual relative infectiousness to be randomly sampled from a gamma distribution with mean 1 but different standard deviations – 0 (i.e. no heterogeneity, the baseline assumption), 0.5, 1, 2 and 4. The impact on the probability of containing an outbreak which would otherwise have been large is shown in Figure SI12. The effect is limited, unless heterogeneity is large (SD=4), in which case, paradoxically, containment is more likely to succeed. This is because if most transmission is due to a few individuals, policies become less sensitive to poor ascertainment – most people generate no secondary infections, whilst the clusters of cases generated by the minority of highly infectious individuals are likely to be detected due to their size.

It should be noted that increasing heterogeneity in infectiousness also increases the probability of spontaneous extinction in the absence of controls; we therefore recalculated baseline extinction probabilities for each of the curves in Figure SI12.

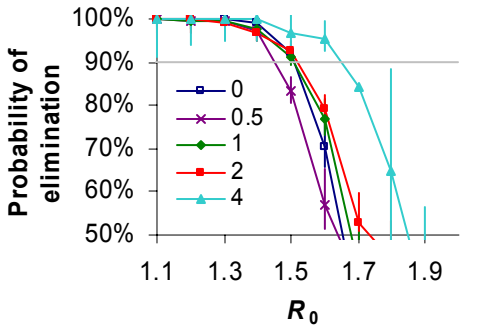

Figure SI12: Effect of varying the degree of variation in infectiousness between individuals, as characterised by the standard deviation of relative infectiousness (mean value being 1). The results in the main text assume no variation (the 0 line). Results assume a 2 day delay from case onset to completion of prophylaxis in the population in the vicinity of each case.. Other parameters as Figure 4d in main text.

Proportion of severe cases

The results in the main text assume 50% of infections result in severe enough disease to make them likely to be detected by surveillance as cases. Figure SI13 shows the impact of varying this assumption on the effectiveness of geographically targeted prophylaxis. Unsurprisingly, increasing the proportion of severe cases increases policy effectiveness (because more infections are detected), while reducing the proportion of severe cases has the opposite impact.

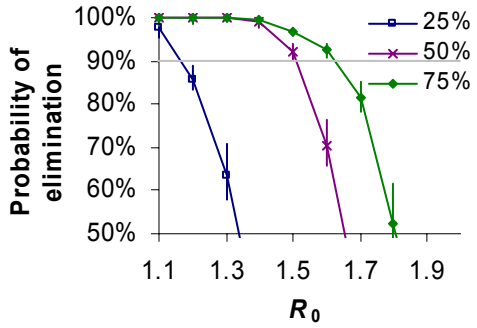

Figure SI13: Effect of varying the proportion of infections which are clinically 'severe': i.e. severe enough to be likely to be detected by surveillance. The results in the main text assume 50% of cases are severe (the 50% line). It is assumed that 90% of severe cases are detected. Other parameters as Figure SI12.

Proportion of cases detected

The results in the main text assumed 90% of severe cases are detected by surveillance. Figure SI14 shows how lowering the proportion of cases detected reduces the effectiveness of containment. The threshold level of R_0 below which 90% containment is achieved scales almost linearly with the proportion of severe cases detected.

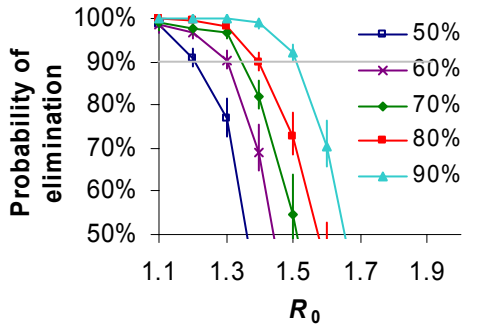

Figure SI14: Effect of varying the proportion of severe cases which are detected by surveillance. The results in the main text assume 90% of severe cases are detected (the 90% line). Other parameters as Figure SI12.

Proportion of population treated

The results in the main text assume social targeting achieves 90% prophylaxis of household members, 90% prophylaxis of 90% of schools/workplaces of cases. Similarly adding geographic targeting implies 90% coverage of everyone within the targeted area. Reducing coverage levels for both social and geographic targeting has a dramatic impact on policy outcome (see Figure SI15). However, it should be noted that reducing coverage only for those targeted by the geographic

component of the policy has a much less significant impact – indicating the maximum possible coverage in households, schools and workplaces is key.

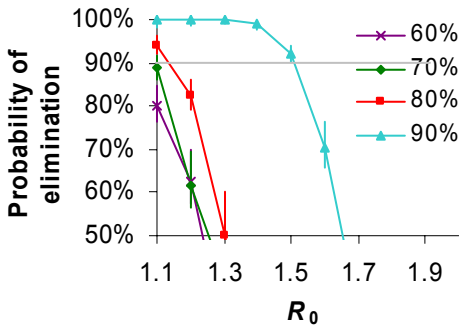

Figure SI15: Effect of varying the proportion of the targeted population who receive prophylaxis. The results in the main text assume 90% coverage. Other parameters as Figure SI12.

Treatment efficacy

Figure SI16 shows the effect of varying assumptions about antiviral efficacy. Policy effectiveness is most sensitive to the extent to which the infectiousness of an individual who is put on prophylaxis prior to infection but still gets infected is reduced. We used a value of 60% reduction in infectiousness estimated from clinical trial data[23], but should this be an underestimate, policy effectiveness could be substantially increased. Similarly, should 60% be an overestimate, policy effectiveness is likely to be much lower than expected. Unfortunately, the data will not exist to estimate antiviral efficacy for any new pandemic strain prior to the introduction of a containment policy.

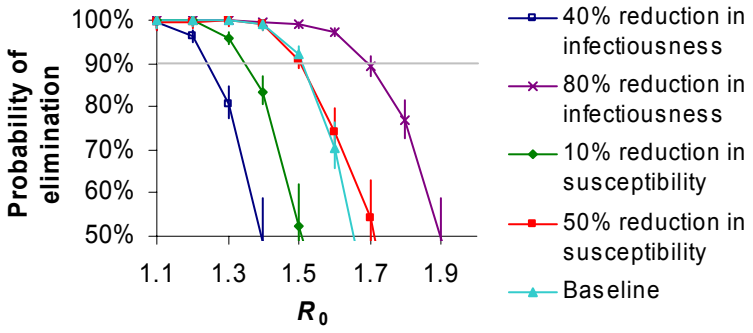

Figure SI16: Effect of varying antiviral efficacy. The baseline assumes prophylaxis reduces susceptibility to infection by 30% and infectiousness by 60%. We vary these 2 parameters separately. Other parameters as Figure SI12.

Age-specific attack rate

The results in the main text assume transmission rates in schools are double that in workplaces, giving rise to a age-specific attack rate profile which is strongly peaked in school age children. We investigated the extent to which the affect policy effectiveness by assuming equal transmission rates in schools and workplaces, and additionally by assuming travel-associated contact rates were constant with age. This produced a flatter age-specific attack rate (not shown), though still one peaked in school children due to the typically large size of schools compared with workplaces and the larger size of households with children. Figure SI17 shows the limited resulting impact on containment probabilities.

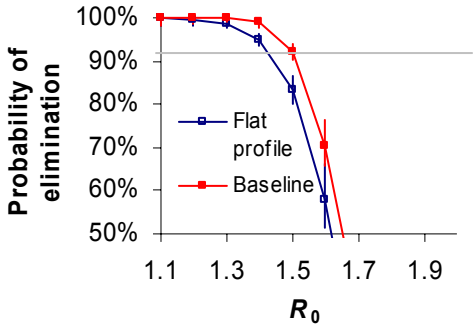

Figure SI17: Effect of varying parameters determining age-specific attack rates. Other parameters as Figure SI12.

Generation time

The results in the main text assume the profile of infectiousness over time given in Figure 1g, resulting in a generation time, T_g ,of 2.6 days. To test the sensitivity of policy effectiveness to this assumption, we undertook simulations assuming infectiousness was constant from end of the latent period for 7 days (giving T_g =4.5 days). The results are shown in Figure SI18. Policy effectiveness is considerably greater if infectiousness is extended, but this has to be balanced against the fact that if the generation time of influenza were as long as 4.5 days, then R_0 estimates derived from historical pandemic data rise from the value of 1.8 used here to of the order of 2.3 (though it should be noted that R_0 =2.3 gives unrealistically high infection attack rates).

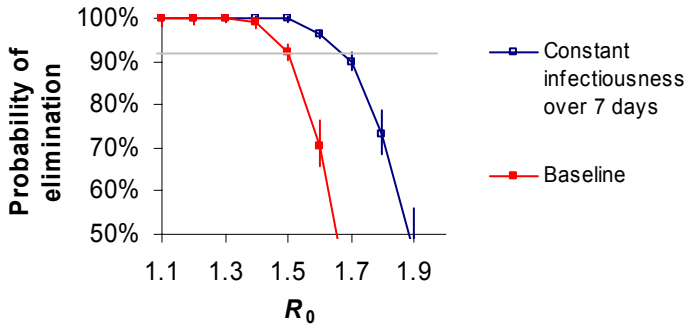

Figure SI18: Effect of varying parameters determining age-specific attack rates. Other parameters as Figure SI12.

False positives

The results above and in the main text assume 100% specificity in case detection; i.e. no false positives. The effect of sub-optimal specificity depends on how false positives arise. If we assumed that clinical (and in a few cases lab-based) screening eliminates false positives with no epidemiological link to existing case clusters, then Figure SI19 shows that the impact of even 1 false-positive per 10 diagnosed cases on policy effectiveness is very limited. However, this results is solely because the spatio-temporal incidence of false positives is assumed to be highly correlated with the incidence of true cases. If the two are uncorrelated (i.e. false positives arise randomly in the whole population), the impact of <100% specificity on policy effectiveness can be very negative. If 10 false positives were to arise each day in the whole population, and each such

case were to trigger local prophylaxis of 10,000 people (typical for the drug-sparing geographic prophylaxis policies), then a stockpile of 3 million courses would be exhausted in 30 days, dramatically reducing the chances of containment. This emphasises the need for cases arising in previously unaffected geographic areas to be investigated as rigorously (but rapidly) as possible.

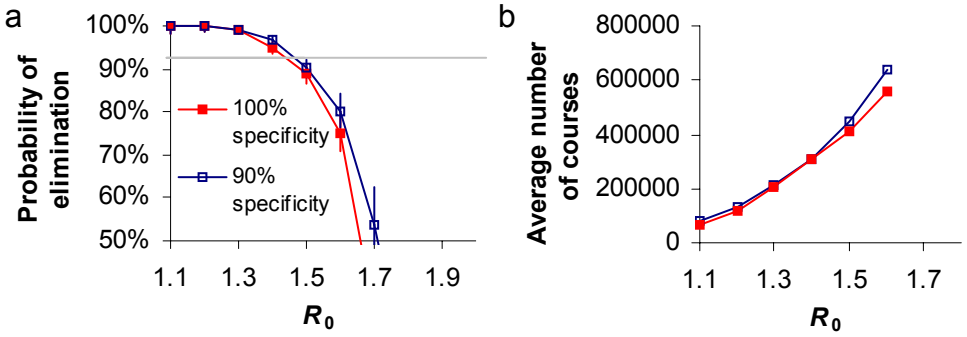

Figure SI19: Effect of <100% specificity in case detection on effectiveness of policy of social prophylaxis + drug-sparing geographic prophylaxis (nearest 20,000 people within 10km of detected case targeted). (a) probability of elimination. (b) average number of drug courses needed for containment. False positives are assumed to arise in contacts of infected individuals at a rate proportional to the rate at which true infections are occurring. Other parameters as Figure SI12.

Urban versus rural seeding

It is interesting to examine the impact spread to urban areas has on policy effectiveness. There is certainly a correlation between policy failure and infection getting into urban centres, but it is unclear whether entering urban centres is a result or a cause of policy failure. As another means of looking at this issue, we therefore examined how policy effectiveness is affected if instead of seeding in rural areas (i.e. having a population density lower than 600/ km^2), we seed infection in high population density areas, here defined as having a population density higher than 6000/km^2 (Figure SI20).

For the pure radial geographic prophylaxis policy (prophylaxing everyone within 5km of a case), the results are superficially surprising (Figure SI20a,b) – urban seeded outbreaks are easier to control. The reason lies in the pattern of population movements assumed (given the gravity model used)– individuals in urban areas tend to travel within that area, typically quite short distances. Individuals in rural areas conversely tend to travel longer distances, perhaps to the nearest town or other villages – many of which may be more than 5km away. The number of courses of drug required for urban control is of course much higher, however.

If one compares the effectiveness of control for urban versus rural seeding for drug-sparing geographic prophylaxis (i.e. targeting the nearest 20,000 people within 10km of each case), then control in urban areas is considerably poorer than in rural areas (Figure SI20c,d)– since in urban areas we end up treating a much smaller fraction of the epidemiological neighbourhood of cases when resource limits are imposed.

Thus one concludes that entry of infection into urban areas is only important for containment for logistical (rather than epidemiological) reasons; i.e. per case detected, many more people will need to be prophylaxed in an urban area, putting huge pressure on policy delivery mechanisms, and exhausting finite stockpiles of drug much more rapidly than would purely rural cases.

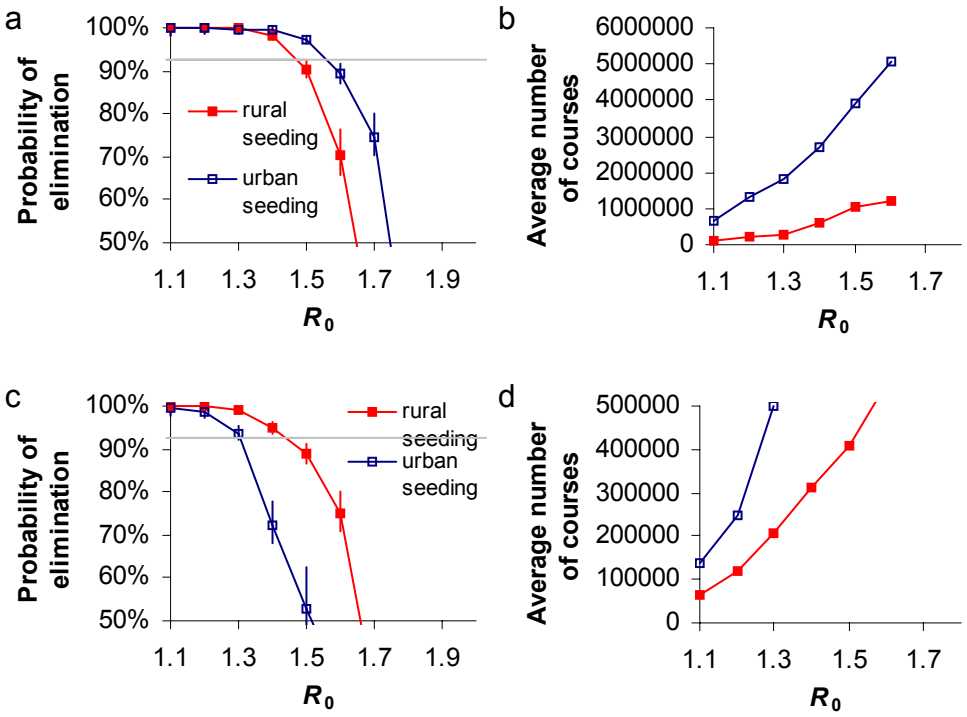

Figure SI20: Effect of seeding in rural vs urban areas. (a) probability of elimination of otherwise large outbreak for policy of social+ pure 5kmn radial prophylaxis (a) probability of elimination. (b) as (a) but showing average number of drug courses needed for containment. (c) as (a) but for social + drug-sparing geographic prophylaxis (nearest 20,000 people within 10km of detected case targeted). (d) as (c) but showing average number of drug courses needed for containment. Other parameters as Figure SI12.

Movement kernel

The transmission model was parameterised with the best available data on journey distances in Thailand. We used a form of gravity model to describe movement patterns, with spatial kernel $f(d) \sim 1/\left[1+(d/a)^b\right]$ where a=4 km and b=3.8. The distribution of travel-to-work distances from the 1991 GB census can be reproduced with a similar gravity model (this time applied to British population density data), with a kernel of the same functional form, but with parameters a=4 km and b=3.0. The parameter b determines how rapidly the kernel decays with distances, and thus the proportion of long distance journeys (smaller b=longer distances). Figure SI21 shows how assuming the Thai population were to show the travel behaviour of the British population (i.e. a longer mean journey distance) substantially reduces policy effectiveness. This illustrates a general result: geographically targeted containment is more effective as population contacts become more localised. This result suggests containment (if able to be implemented) might be more successful in countries such as Vietnam, Cambodia and Laos, given the transport infrastructures of those countries are less developed than that of Thailand and thus mean journey distances are likely to be shorter.

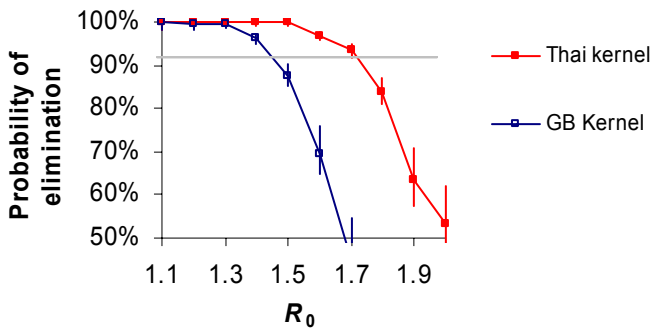

Figure SI21: Effect of different movement kernels on the effectiveness of a policy of social prophylaxis + drug-sparing geographic prophylaxis (nearest 50,000 people within 10km of detected case targeted) + 5km area quarantine applied to a pandemic outbreak originating in Thailand. Results assume a stockpile of 3 million drug courses is available. Other parameters as Figure SI12.

Evolution of transmissibility

It is not certain whether transmissibility of a pandemic virus strain will evolve incrementally (with R_0 starting just above 1, and gradually increasing), or in a single discrete step (e.g. to R_0 ~1.8 via reassortment). We have focussed on the latter scenario in the main text, as that poses most challenges to containment. However, here we specifically examine containment of an virus strain with evolving transmissibility.

We model a strain which has an initial R_0 value between 1 and 2, but which can double its transmissibility via mutation. We assume single mutations increase R_0 by 20% or 50% of the initial value (meaning 5 or 2 mutations are needed to double R_0 respectively), and that there is a 1% probability per day of infection per infected person of a mutation causing the virus in that person to increase its transmissibility. Such a mutation rate is almost certainly a gross overestimate, given the estimates of net mutation rates one obtains from examining genetic evolution of interpandemic flu A.

The effect of the possibility of mutation on containment probabilities is remarkably slight (Figure SI22) – meaning that in essence, containment policies should be targeted at the initial R_0 value. The reason for this is that successful containment policies tend to eliminate the virus when the outbreak is still small (i.e. before than 150 cases or 300 infections have arisen), meaning the probability that mutations arise to increase transmissibility is small.

These results imply that under the scenario of incrementally evolving transmissibility, relatively low-intensity control measures (such as purely socially targeted prophylaxis) might have a high probability of success (though it has to be born in mind that a low R_0 outbreak has a high chance of spontaneously going extinct). This is of course encouraging, but we would still always urge that planning be for the worst case – if R_0 is low and an intensive policy is adopted, the outbreak will be eliminated very rapidly, minimising cost in any case (e.g. for R_0 =1.4, the drug-sparing geographic prophylaxis strategy would use ~200,000 courses to contain an outbreak – less than 10% of the envisaged WHO international stockpile).

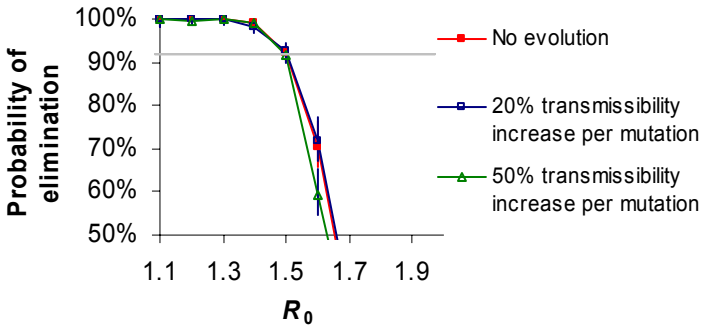

Figure SI22: Effect of allowing transmissibility to evolve. There is a 1% probability of a mutation arising which increases transmissibility per infected individual per day (see text above). Other parameters as Figure SI12. For evolution of transmissibility to play a significant role, the probability of evolution per individual per day needs to be of the order of 10% - much larger than is feasible.

4. Bibliography

1. Oakridge National Laboratory. Landscan global population data. http://www.ornl.gov/sci/gist/landscan (2003).
2. National Statistical Office Thailand. Population and Labor Statistics. http://www.nso.go.th/eng/stat/subject/subject.htm#cata1 (1999).
3. National Statistical Office Thailand. Population Census 2000. http://www.nso.go.th/pop2000/pop_e2000.htm (2000).
4. National Statistical Office Thailand. Education and Public Health Statistics. http://www.nso.go.th/eng/stat/subject/subject.htm#cata6 (1999).
5. Ministry of Education Thailand. Class size data for Thai schools. http://www.moe.go.th/ (2005).
6. Faust, K., Entwisle, B., Rindfuss, R. R., Walsh, S. J. & Sawangdee, Y. Spatial arrangement of social and economic networks among villages in Nang Rong District, Thailand. *Social Networks* **21**, 311–337 (1999).
7. Ministry of Labour Thailand. Yearbook of Labour Statistics. http://www1.mol.go.th/download/chap031-2.pdf (2003).
8. Axtell, R. L. Zipf Distribution of U.S. Firm Sizes. *Science* **293**, 1818-1820 (2001).
9. Chamratrithirong, A. et al. National Migration Survey of Thailand. (Institute for Population and Social Research, Mahidol University, Bangkok, 1995).
10. Xia, Y., Bjornstad, O. N. & Grenfell, B. T. Measles metapopulation dynamics: a gravity model for epidemiological coupling and dynamics. *Am Nat* **164**, 267-81 (2004).
11. Ortuzar, J. & Willumsen, L. G. *Modelling Transport: Third Edition* (Wiley, Chichester, 2001).
12. Wong, C. M., Chan, K. P., Hedley, A. J. & Peiris, J. S. Influenza-associated mortality in Hong Kong. *Clin Infect Dis* **39**, 1611-7 (2004).
13. Simmerman, J. M. et al. Influenza in Thailand: a case study for middle income countries. *Vaccine* **23**, 182-7 (2004).
14. Elveback, L. R. et al. An influenza simulation model for immunization studies. *Am J Epidemiol* **103**, 152-165 (1976).
15. Rvachev, L. A. & Longini, I. M. A Mathematical-Model for the Global Spread of Influenza. *Mathematical Biosciences* **75**, 3-23 (1985).
16. Moser, M. R. et al. An outbreak of influenza aboard a commercial airliner. *American Journal of Epidemiology* **110**, 1-6 (1979).
17. Cauchemez, S., Carrat, F., Viboud, C., Valleron, A. J. & Boelle, P. Y. A Bayesian MCMC approach to study transmission of influenza: application to household longitudinal data. *Statistics in Medicine* **23**, 3469-3487 (2004).
18. Carrat, F. et al. Influenza burden of illness: estimates from a national prospective survey of household contacts in France. *Arch Intern Med* **162**, 1842-8 (2002).
19. Longini, I. M., Jr., Koopman, J. S., Haber, M. & Cotsonis, G. A. Statistical inference for infectious diseases. Risk-specific household and community transmission parameters. *Am J Epidemiol* **128**, 845-59 (1988).
20. Mills, C. E., Robins, J. M. & Lipsitch, M. Transmissibility of 1918 pandemic influenza. *Nature* **432**, 904-6 (2004).
21. HMSO. Forty-Eighth Annual Report of the Local Government Board, 1918-19. Supplement Containing the Report of the Medical Officer for 1918-19. 24-27 (London, 1919).
22. Stuart-Harris, C. H. Pandemic influenza: an unresolved problem in prevention. *J Infect Dis* **122**, 108-15 (1970).
23. Yang, Y. & Longini, I. M. New Methods for the Estimation of Influenza Antiviral Agent Efficacy. in *Joint Statistical Meetings* (San Francisco, 2003).